Field direction dependent quantum-limit magnetoresistance of correlated Dirac electrons in perovskite math xmlns="http://www.w3.org/1998/Math/MathML">msub>mi>CaIrO/mi>mn>3/mn>/msub>/math>

Rinsuke Yamada, Jun Fujioka, Minoru Kawamura, Shiro Sakai, Motoaki Hirayama, Ryotaro Arita, Tatsuya Okawa, Daisuke Hashizume, Ryosuke Kurihara, Masashi Tokunaga, and Yoshinori Tokura

Phys. Rev. B **107**, L081113 — Published 22 February 2023

DOI: 10.1103/PhysRevB.107.L081113

Field-direction dependent quantum-limit magnetoresistance of correlated Dirac electrons in perovskite $CaIrO_3$

Rinsuke Yamada[1], Jun Fujioka[2], Minoru Kawamura[3], Shiro Sakai[3], Motoaki Hirayama[1,3], Ryotaro Arita[3,4], Tatsuya Okawa[1], Daisuke Hashizume[3], Ryosuke Kurihara[5], Masashi Tokunaga[5], and Yoshinori Tokura[1,3,6]

[1] *Department of Applied Physics, University of Tokyo, Tokyo 113-8656, Japan*
[2] *Division of Materials Science, University of Tsukuba, Tsukuba 305-8573, Japan*
[3] *RIKEN Center for Emergent Matter Science (CEMS), Wako 351-0198, Japan*
[4] *Research Center for Advanced Science and Technology, University of Tokyo, Tokyo 153-8904, Japan*
[5] *The Institute for Solid State Physics, University of Tokyo, Kashiwa 277-8581, Japan*
[6] *Tokyo College, University of Tokyo, Tokyo 113-8656, Japan*

(Dated: February 9, 2023)

Correlated-electron perovskite $CaIrO_3$ shows the topologically protected line node near the Fermi level, wherein the high-mobility Dirac electrons reach the quantum-limit (QL) with the one-dimensionally (1D) dispersive n=0 Landau level (LL) state at a moderate magnetic field. In the QL, the longitudinal magnetoresistance (MR) shows an extreme anisotropy against the field (B) direction in spite of nearly isotropic Dirac band dispersions. The resistivity for $B \parallel a$ shows an insulating behavior with the MR ratio exceeding 2000 % around 18 T, whereas the $B \parallel c$ MR always remains metallic. This is accounted for in terms of that the large difference of Fermi velocity of the n=0 LL between $B \parallel a$ and $B \parallel c$ due to the B-direction dependent 5d orbital electron hopping, which triggers the different instability toward the charge density wave formation for the 1D ($\parallel B$) dispersive n=0 LL.

INTRODUCTION

The quantum phenomena of relativistic electrons in solids have received significant interest in modern condensed matter physics. In topological semimetals, the bulk electronic state possesses the band crossing points or lines protected by the symmetry [1, 2], which is effectively described by the relativistic electron (Dirac and Weyl fermion) and often shows various quantum transport phenomena [3]. A remarkable feature of relativistic electron is that the Landau quantization occur at a moderate magnetic field (B) due to the extremely small transport mass. In particular, in the quantum limit (QL), the electrons in the lowest index of Landau levels (LLs) are confined into the quasi-one dimensional state, which often causes collective quantum phenomena due to the Fermi surface instability or electron correlation effect [4–7]. For example, recent studies argue the possible realization of axionic charge density wave, Wigner crystallization, or excitonic insulator in the QL of topological semimetals [8–15]. Since the electronic ordering is generally sensitive to the details of electronic structure such as the Fermi surface topology or Fermi energy (E_F) , the QL transport can be dramatically varied by manipulating the LL structure.

One of the promising candidates to study this issue is the correlated Dirac semimetallic perovskite $CaIrO_3$, in which the metal-insulator crossover is triggered by the collective electronic ordering, such as the charge/spin density wave (CDW/SDW) , in the QL [16, 17]. The crystal structure of the perovskite $CaIrO_3$ has an orthorhombic $GdFeO_3$-type distortion [see Fig. 1(a)]. Theoretical studies show that the electronic state close to E_F is composed of a nearly half-filled J_{eff}= 1/2 multiplet of Ir^{4+} 5d orbitals that constitutes the nodal line protected by orthorhombic crystal symmetry [see Fig. 1(b)] [18–22] around the U-point in the momentum space [see the inset to Fig. 1(d)]. In particular, the line node is likely located only 10 meV below E_F due to the strong electron correlation effect, resulting in the Dirac semimetal with high electron mobility and dilute carrier density [16, 23]. As a result, the Dirac electron reaches the QL at a moderate field of 6 T (=B_{QL}) for $B \parallel a$. Figure 1(d) shows the magnetoresistivity (MR) in the longitudinal configuration, where both the magnetic field and electric current are applied along the a-axis of the orthorhombic perovskite structure ($B \parallel I \parallel a$, ρ_a) [17, 24]. In the QL region above 10 T, ρ_a steeply increases by more than one order of magnitude and shows a giant peak around 18 T with the MR-ratio of 2,600 % at 2 K. This conspicuous positive MR was ascribed to the emergence of collective electronic ordering, such as CDW/SDW promoted by the quasi-one-dimensional confinement of Dirac electrons in the QL [17].

From the symmetry argument, the theoretical study predicts that the electronic state can be significantly controlled by changing B-direction regardless of small anisotropic band dispersion around the line node: the Fermi velocity (v_F) along k_a is only about 30 % smaller than that along k_c [see Figs. 1(b) and 1(c)] [25]. However, such anisotropic behavior has not been experimentally observed [16]. Here, by magneto-transport measurements and numerical calculations, we show that the MR of correlated Dirac electrons shows large field-directional anisotropy in the QL. Contrary to the field-induced insulating state originating from the possible density wave formation for $B \parallel a$ [17], the metallic state

remains in the QL for $B \parallel c$. The theoretical calculation suggests that $v_{\rm F}$ of the lowest LLs substantially decreases due to the reduction of intra-orbital electron hopping for $B \parallel c$, hindering the evolution of electronic ordering, whereas it does not significantly change for $B \parallel a$. It is likely that the density wave formation in the QL of $CaIrO_3$ can be controlled by varying the B-direction.

METHODS

Single crystals of perovskite $CaIrO_3$ were synthesized under high pressure using a cubic anvil-type apparatus, as described in detail elsewhere [16]. The sample was kept at 1 GPa and 1300 °C for 30 minutes, and then quenched to room temperature. The resistivity was measured by a standard four-probe method. We used two different samples S9 and LK12 to measure the MR for $B \parallel I \parallel a$ and $B \parallel I \parallel c$, respectively [see Supplementary Materials [24]]. We construct a low-energy effective model to describe the electronic structure around the line node [19, 26] and derived the LLs by the numerical calculation.

RESULTS AND DISCUSSION

Large anisotropy in the magnetoresistance.

Figure 1(e) shows the MR for $B \parallel I \parallel c$ (ρ_c). At 2 K, ρ_c initially increases in the low B region below 1 T and shows a small peak around 2 T. Looking closely at ρ_c below 1 T, the MR shows the weak beating pattern due to the Shubnikov-de-Haas (SdH) oscillations [16]. From the analysis of the oscillating part of MR as shown in the inset to Fig. 1(e), the QL is revealed to be reached at the magnetic field ($B_{\rm QL}$) as small as 1 T, which nearly corresponds to the small MR peak [see also Supplementary Materials [24]]. It should be noted that $B_{\rm QL}$ for $B \parallel c$ is about 1/6 of that for $B \parallel a$. By sweeping B above $B_{\rm QL}$, ρ_c shows a dip around 2 T and then a broad peak around 6 T with the MR-ratio of 260 %. Although the appearance of a peak in the quantum limit is common between ρ_c and ρ_a, the peak of ρ_c appears at a lower B (6 T) than that of ρ_a (18 T), and its magnitude is much smaller. With increasing temperature (T), the peak structure of ρ_a around 18 T is suppressed due to the thermally induced blurring of the LLs [17]. Similarly, both the SdH oscillations and small/broad peaks in ρ_c gradually diminish, which are no longer discernible above 15 K. In particular, the resistivity monotonically decreases with B above 2 T, which may be ascribed to the chiral anomaly [27] or current jetting effect [28] [see Supplementary Materials [24]].

The anisotropy can be clearly seen in the temperature-field profiles of ρ_a and ρ_c as shown in Figs. 2(a) and (b). ρ_a shows a large peak structure at low T, and the resistivity at the peak of 18 T shows the clear insulating T dependence [see Figs. 2(a) and (c)] due to the evolution of electronic ordering [17]. On the other hand, the broad peak of ρ_c around 6 T does not show an insulating behavior [see Figs. 2(b) and (d)]. This suggests that the evolution of electronic ordering is strongly suppressed for $B \parallel c$, in contrast with the case of $B \parallel a$. Despite the different T dependence nearby the peak of MR, at high B, both of ρ_a and ρ_c show a similar weak T dependence described by the power-law type function, which is consistent with the picture of Tomonaga-Luttinger liquid [29, 30] [see Supplementary Materials [24]].

Anisotropy in Landau levels of the line node

Considering that the shape of the line node and $v_{\rm F}$ is nearly isotropic on the k_a-k_c plane [16, 23], the large anisotropy of the quantum-limit MR between for $B \parallel a$ and $B \parallel c$ is surprising. To understand the origin of the anisotropic behavior in the QL, we explored the LL structures nearby the line node both for $B \parallel a$ and $B \parallel c$ by the model calculation [see Fig. 3].

The low-energy electronic state around the U-point near $E_{\rm F}$ is modeled by the effective Hamiltonian that respects the orthorhombic symmetry [25, 26],

$$H = 2t_0 k_b \tau_x - t_0 k_c \nu_x - t_1 k_b \tau_y \sigma_z - \frac{1}{2} t_3 k_a \nu_z \tau_y (\sigma_x + \sigma_y) + \frac{1}{2} t_2 k_c \nu_y \tau_z (\sigma_x - \sigma_y) - \frac{1}{2} t_4 k_b \nu_z \tau_y (\sigma_x - \sigma_y) + t_5 \nu_x \tau_y (\sigma_x - \sigma_y), \quad (1)$$

where the origin of $\boldsymbol{k} = (k_a, k_b, k_c)$ is set to the U-point in the momentum space. σ_α ($\alpha = a, b, c$) is the Pauli matrix with respect to the Kramers doublet of $J_{\rm eff}$= 1/2 state, while τ_α and ν_α are those for the pseudo-spins representing the four Ir sublattices inherent to the orthorhombic perovskite structure [31]. The first two terms represent the nearest neighbor Ir-Ir hopping via the intra-orbital hybridization (e.g. d_{xy}-d_{xy}), which are the high symmetry terms allowed even in the cubic perovskite structure. On the contrary, the third, fourth, and subsequent terms are nearest neighbor Ir-Ir hopping via the inter-orbital hybridization (e.g. d_{xy}-d_{yz}), which are allowed by the tilting or rotation of IrO_6 octahedra due to the orthorhombic lattice distortion. In particular, these terms represent the coupling between pseudospin of sublattice and $J_{\rm eff}$=1/2 state, which can be viewed as the "intersite spin-orbit coupling". We chose parameters (t_0-t_5) so as to reproduce the experimental observations and band calculations [see Supplementary Materials [24]].

Figures 3(a)-(d) and 3(f)-(i) show the calculated electronic structure plotted as a function of k_a and k_c for $B \parallel a$ and $B \parallel c$, respectively. At 0 T, two branches cross at E=0 eV, corresponding to the nodal line [see Figs. 3(a) and 3(f)]. The dispersion along k_a is merely by 30 % smaller than that along k_c, and the difference is not significant. Nevertheless, under B, the electronic structure becomes significantly anisotropic between for $B \parallel a$ and $B \parallel c$, as presented below. For $B \parallel a$, the LLs with monotonic energy dispersion are formed, and the energy splitting between them increases with B, as shown in Figs. 3(b)-(d). The n=0 LLs are composed of nearly degenerate two branches and cross at k_a=0 irrespective of the magnitude of B, which corresponds to the double Weyl points [17]. Note that the Fermi velocity of n=0 LLs ($v_{\rm F}^{\rm QL}$) slightly decreases under B, but is nearly comparable with that at B = 0 T. On the contrary, for $B \parallel c$, the LLs ($n \neq 0$) show wiggled energy dispersion and the energy splitting between them appears to be much larger than the case of $B \parallel a$ [see Figs. 3(g)-(i)]. The two branches of n=0 LLs are nearly degenerate, but cross each other at non-zero k_c [see the insets to Figs. 3(h) and 3(i)], which increases as a function of B. The B-directional dependence of band crossing point may originate from the difference in band topology under the magnetic field as shown in Ref. [19]. Note that the $v_{\rm F}^{\rm QL}$ for $B \parallel c$ is less than 1/2 of that at 0 T and consequently about 2.4 times smaller than that for $B \parallel a$.

Here we assume that $E_{\rm F}$ is located at around 5 meV above the line node in the low B region ($B < B_{\rm QL}$) as shown in Figs. 3(a) and 3(e) [17]. The cross-sections of the Fermi surface with $E_{\rm F}$ = 5 meV at k_a = 0 and k_c = 0 are shown in Figs. 3(e) and 3(j), respectively. The cross-section at k_a = 0 with a "butterfly-type" shape has about 5 times larger area than that at k_c = 0 with an elliptical shape; this is consistent with the anisotropy of extremal cross-sectional area of Fermi surface derived from SdH oscillations [16]. Furthermore, the calculated $B_{\rm QL}$ is around 6 T (2 T) for $B \parallel a$ ($B \parallel c$) in agreement with the experimental results. With increasing B, the Landau degeneracy is enhanced, and thus $E_{\rm F}$ decreases in proportion to $1/B$ in the QL, given that the carrier density of the Dirac band is conserved. More specifically, given that the two branches of n=0 modes are regarded as the degenerate state, $E_{\rm F}$ would be roughly given by $\hbar v_{\rm F}^{\rm QL} k_{\rm F}^{\rm QL}$. Here, $k_{\rm F}^{\rm QL}$ is the Fermi wave number along B in the QL. Considering that $k_{\rm F}^{\rm QL}$ is nearly of the same magnitude for $B \parallel a$ and $B \parallel c$ in the QL, $E_{\rm F}$ for $B \parallel c$ is 2.4 times smaller than that for $B \parallel a$ due to the smaller $v_{\rm F}^{\rm QL}$ along k_c [see and compare Figs. 3(d) and 3(i)].

To understand the origin of anisotropy of the LLs between $B \parallel a$ and $B \parallel c$, we consider the relation between $v_{\rm F}$ and inter-site electron hopping represented by each term of Eq. (1) under B. Eq. (1) suggests that the dispersion along k_a is determined only by the inter-orbital hybridization (fourth-term). The absence of contribution from the intra-orbital hybridization is a consequence of interference of electron hopping in the orthorhombic crystal structure [26]. The fact that $v_{\rm F}$ does not significantly change under B means that the electron hopping via these inter-orbital hybridization terms is not sensitive to the electronic state reconstruction upon the Landau quantization for $B \parallel a$. On the other hand, the dispersion along k_c is determined by both the intra-orbital hybridization (second-term) and inter-orbital hybridization (fifth-term). Indeed, these terms contribute with nearly comparable weight at B=0 T. The reduction of $v_{\rm F}$ for $B \parallel c$ under B [see Figs. 3(f)-(i)] may indicate that the contribution from these two terms changes when the LLs are formed. To clarify this point, we calculated LLs by changing the relative weight of these terms while keeping $v_{\rm F}$ at B=0 T constant [see Supplemental Materials [24]]. The calculated result shows that the $v_{\rm F}^{\rm QL}$ is almost determined by the inter-orbital hybridization term (fifth-term) rather than by the intra-orbital hybridization term (second-term). In other words, it is likely that the reconstruction of the orbital state due to the Landau quantization selectively reduces the contribution from the intra-orbital hybridization terms (high symmetry terms), resulting in the reduction of $v_{\rm F}$ under B. Such a B-direction sensitive electronic state in the QL due to the orbital-dependent electron hopping has not been observed in the conventional Dirac semimetal with the nearly s- or p-orbital character, which may highlight the feature of d-electron Dirac semimetal [32, 33].

Gap size of CDW for $B \parallel a$ and $B \parallel c$

Having established the origin of B-directional anisotropy of LLs, we discuss the origin of the anisotropic MR in the QL. The recent study demonstrated that the insulating behavior for $B \parallel a$ can be well understood by the field-induced CDW/SDW [17]. Although the type of density wave has not been uniquely determined, here we assume the charge density wave (CDW) as a plausible electronic state and calculated the transition temperature T_C as well as the charge gap Δ_{cal} following the mean-field theory [4, 24]. We show the B-dependence of Δ_{cal} for $B \parallel a$ in Fig. 4(b), which is reproduced from Ref. [17]. For $B \parallel a$, Δ_{cal} initially increases as a function of B, shows a maximum around 15 T, and gradually decreases at higher B, which is in accord with B-dependence of ρ_a. To calculate Δ_{cal} for $B \parallel c$, v_F and E_F are set to be 2.4 times smaller than those for $B \parallel a$, while k_F is set to the same value, on the basis of the aforementioned numerical calculation of LLs. As shown in Fig. 4(b), the B-dependence of Δ_{cal} for $B \parallel c$ shows a peak around 10 T, and the peak value is smaller than that for $B \parallel a$. The smaller peak field and peak height for $B \parallel c$ qualitatively agree with the experimental results [see Fig. 4(a)].

We note here that the peak height of MR appears to be more anisotropic than that of Δ_{cal}; the peak of ρ_c is about one order smaller than that of ρ_a, while the Δ_{cal} for $B \parallel c$ is only by 30 % smaller than that for $B \parallel a$. Indeed, MR-peak for $B \parallel c$ does not clearly show the thermal activation type dependence [see also Fig. 2(b)] and hence no clear feature of gap-opening is discerned. One possible reason for this discrepancy is that the present analysis is based on the mean-field theory and does not consider the effect of randomness that may suppress the long-range density-wave order; this effect will be pronounced at a higher B that causes a lower k_F state of the n=0 LL [see Fig. 3] [17]. Another factor may be the inaccurate modeling of the dielectric screening due to the lattice polarization or interband/intraband electronic excitation in the ordered state. Despite the discrepancy at a quantitative level, the qualitative agreement between the experimental result and model calculation suggests that the variation of LL structure with the field direction significantly affects the evolution of electronic ordering and magnetoresistivity in the QL. Such a large field-direction sensitive behavior likely originates from the Ir 5d orbital electron hopping and the formation of density wave in the QL, which are charctersitc of the present material.

CONCLUSION

In summary, we have investigated the field-direction dependence of quantum limit magnetoresistivity (MR) in the Dirac semimetal of perovskite $CaIrO_3$. The MR for $B \parallel a$ shows a giant positive MR with the insulating temperature dependence due to the collective electronic ordering, such as the charge density wave, whereas that for $B \parallel c$ shows moderate field dependence and remains metallic even at the lowest temperature. The numerical calculation of the Landau levels demonstrates that although the Dirac band dispersion nearby the line node is nearly isotropic on the k_a-k_c plane at zero magnetic field, the Fermi velocity of the n=0 Landau level for $B \parallel c$ becomes 2.4 times smaller than that for $B \parallel a$ due to the field-direction dependent reduction of intra-orbital electron hopping under B. Due to the reduced Fermi velocity, or equivalently to the Fermi energy, the field-induced evolution of the density wave is likely suppressed for $B \parallel c$, resulting in the large field-directional dependence of quantum-limit MR in the present material.

ACKNOWLEDGEMENT

Authors thank A. Tsukazaki, M. Kawasaki, N. Nagaosa, A Yamamoto, Y. Kaneko, S. Ishiwata, Y. Fuseya, Y. Awashima, M. Masuko, and R. Kaneko for fruitful discussion. This work was supported by a Japan Society for the Promotion of Science KAKENHI (Grants 22H01177, 21K18813, No. 20J21312, No. 18H01171, No. 18H04214, No. 16H00981, and No. 16H06345) from the MEXT and by PRESTO (Grant No. JPMJPR15R5) and CREST (Grants No. JPMJCR16F1), Japan Science and Technology Japan.

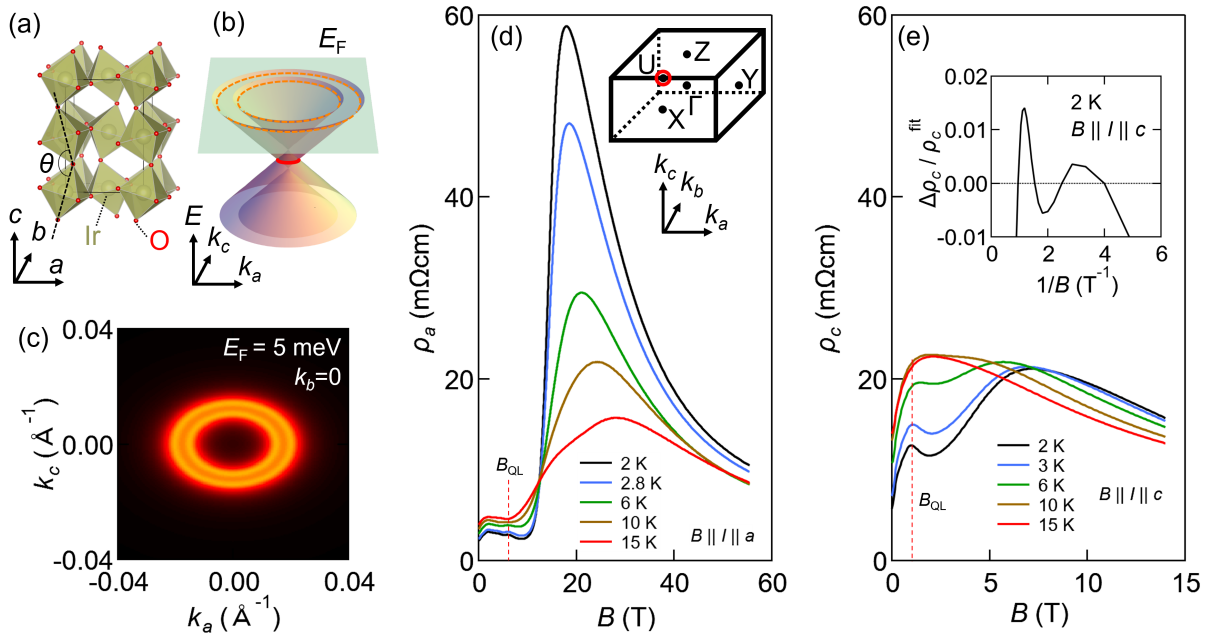

Fig. 1: Large anisotropy in the magnetoresistance (MR). (a) Crystal structure of orthorhombic perovskite $CaIrO_3$. The perovskite structure is distorted so that the average Ir-O-Ir angle (θ) is smaller than 180°. (b) Illustration of Dirac-like band dispersion around line node (red solid line). The pale green plane shows Fermi energy (E_F) and the dotted orange lines indicates inner- and outer-Fermi surface. (c) The cross-section of Fermi surface derived from the tight binding model (see the text). Here, we set $E_F = 5$ meV above the line node and defined the origin of k as the U-point. (d) MR for $B \parallel I \parallel a$ (ρ_a) at various temperatures, which is reproduced from Ref. [17]. The inset shows the position of the line node (red circle) in Brillouin zone. (e) MR for $B \parallel I \parallel c$ (ρ_c) at various temperatures. The inset shows the oscillatory component plotted against $1/B$ for $B \parallel c$ at 2 K. Red dotted lines in (d) and (e) represents the magnetic field where Dirac electrons reach quantum limit (B_{QL}).

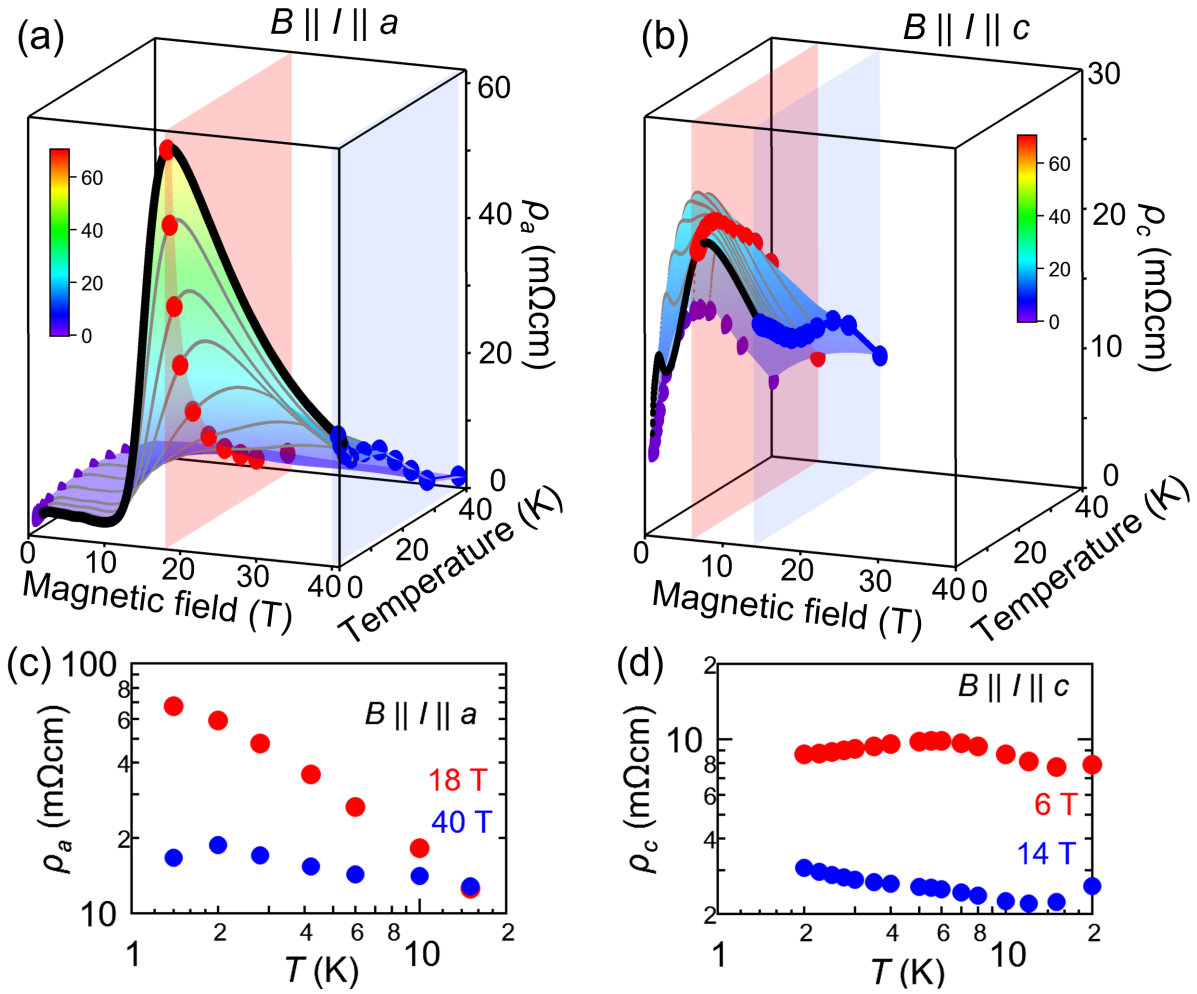

Fig. 2: Comparison of the MR for $B \parallel I \parallel a$ (ρ_a) and $B \parallel I \parallel c$ (ρ_c). (a), (b) Temperature- and field-dependence of ρ_a (sample S9) and ρ_c (sample LK12). The purple, red, and blue points in (a) show temperature dependence of ρ_a at 0, 18, 40 T, respectively, while those in (b) show that for ρ_c at 0, 6, 14 T, respectively. (c), (d) The detailed temperature dependence of ρ_a and ρ_c below 20 K at the magnetic field where the peak appears in the MR (18 T and 6 T, respectively) as well as at the enough higher field (40 T and 14 T, respectively). The resistivity ρ_a in (a,c) is reproduced from Ref. [17].

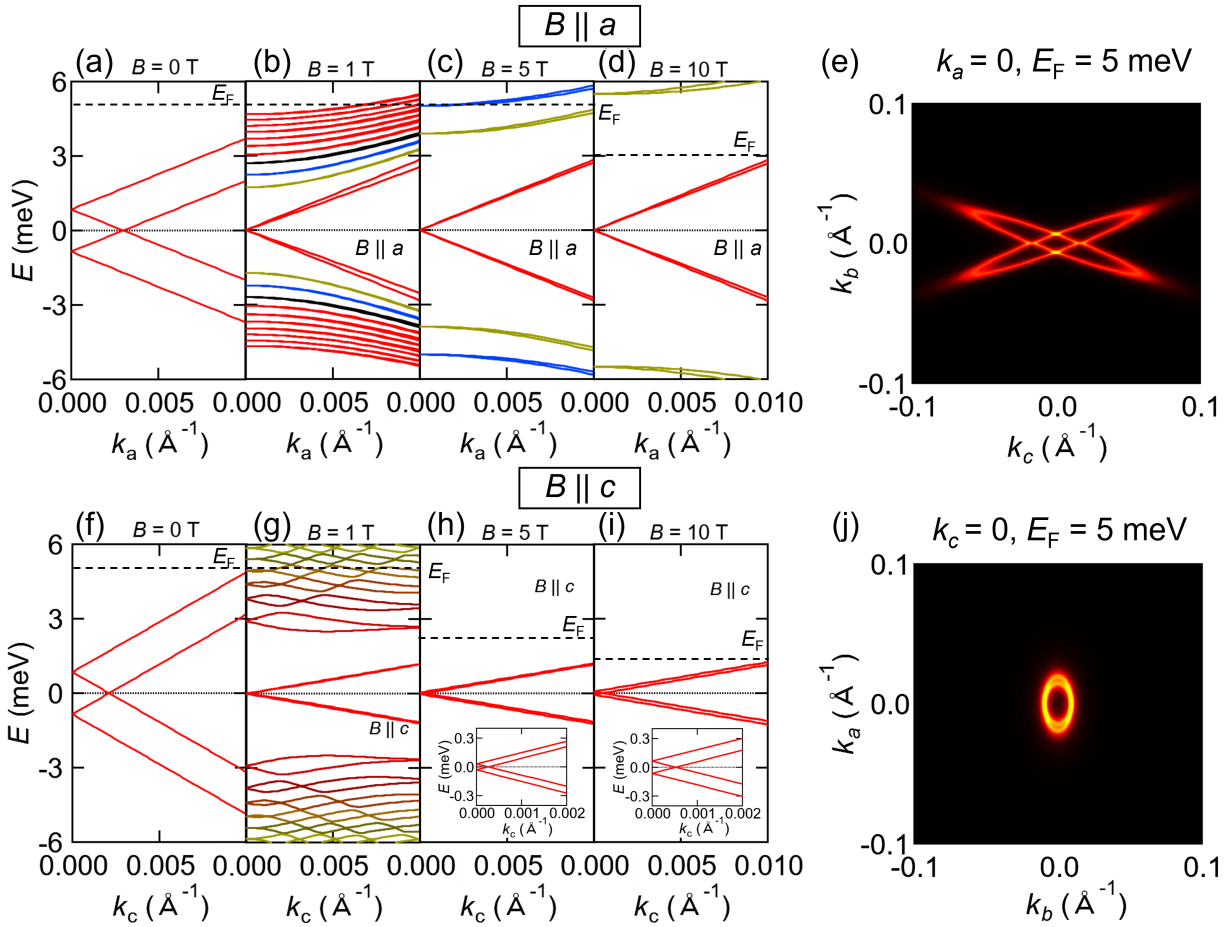

Fig. 3: Field-direction dependent formation of the Landau levels (LLs) of the line node in $CaIrO_3$. (a), (f) Calculated energy dispersion near the line node along k_a- and k_c-direction ($B = 0$), respectively. (b)-(d) The LLs of the line node for $B \parallel a$ at $B = 1$, 5, and 10 T, respectively. (g)-(i) The LLs of the line node for $B \parallel c$ at $B = 1$, 5, and 10 T, respectively. (e), (j) The cross-section of Fermi surface ($B = 0$) with $E_F = 5$ meV above the line node on the k_a=0-plane and k_c=0-plane, respectively. The insets to (h) and (i) show the magnified view in the low energy regime.

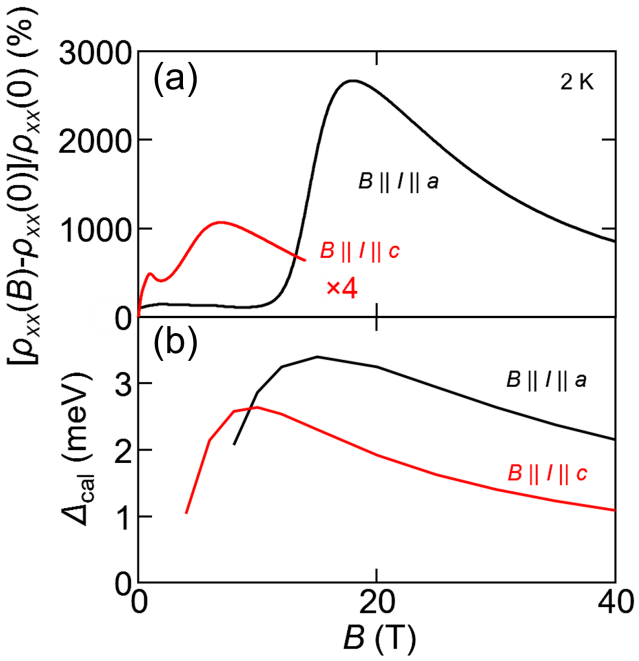

Fig. 4: Suppression of CDW formation in the QL for $B \parallel c$. (a) MR ratio for $B \parallel I \parallel a$ (black line, Ref. [17]) and $B \parallel I \parallel c$ magnified by a factor of 4 (red line). (b) The gap size of CDW as calculated for $B \parallel a$ (black line, Ref. [17]) and $B \parallel c$ (red line).

[1] N. P. Armitage, E. J. Mele, and A. Vishwanath, Rev. Mod. Phys. **90**, 015001 (2018).
[2] A. Bernevig, H. Weng, Z. Fang, and X. Dai, J. Phys. Soc. Japan **87**, 041001 (2018).
[3] N. Nagaosa, T. Morimoto, and Y. Tokura, Nat. Rev. Mater. **5**, 621 (2020).
[4] H. Fukuyama, Solid State Commun **26**, 783 (1978).
[5] Y. Iye, P. M. Tedrow, G. Timp, M. Shayegan, M. S. Dresselhaus, G. Dresselhaus, A. Furukawa, and S. Tanuma, Phys. Rev. B **25**, 5478 (1982).
[6] L. Li, J. G. Checkelsky, Y. S. Hor, C. Uher, A. F. Hebard, R. J. Cava, and N. P. Ong, Science **321**, 547 (2008).
[7] K. Behnia, L. Balicas, and Y. Kopelevich, Science **317**, 1729 (2007).
[8] K.-Y. Yang, Y.-M. Lu, and Y. Ran, Phys. Rev. B **84**, 075129 (2011).
[9] Z. Wang, Y. Sun, X.-Q. Chen, C. Franchini, G. Xu, H. Weng, X. Dai, and Z. Fang, Phys. Rev. B **85**, 195320 (2012).
[10] B. Roy, J. Hofmann, V. Stanev, J. Sau, and V. Galitski, Phys. Rev. B **92**, 245431 (2015).
[11] C.-L. Zhang, B. Tong, Z. Yuan, Z. Lin, J. Wang, J. Zhang, C.-Y. Xi, Z. Wang, S. Jia, and C. Zhang, Phys. Rev. B **94**, 205120 (2016).
[12] B. J. Ramshaw, K. Modic, A. Shekhter, Y. Zhang, E. Kim, P. Moll, M. Bachmann, M. Chan, J. Betts, F. Balakirev, A. Migliori, N. Ghimire, E. Bauer, F. Ronning, and M. R., Nat. Commun. **9**, 2217 (2018).
[13] H. Wang, H. Liu, Y. Li, Y. Liu, J. Wang, J. Liu, J.-Y. Dai, Y. Wang, L. Li, J. Yan, D. Mandrus, X. C. Xie, and J. Wang, Sci. Adv. **4**, eaau5096 (2018).
[14] F. Tang, Y. Ren, P. Wang, R. Zhong, J. Schneeloch, S. A. Yang, K. Yang, P. A. Lee, G. Gu, Z. Qiao, and L. Zhang, Nature **569**, 537 (2019).
[15] J. M. Ok, N. Mohanta, J. Zhang, S. Yoon, S. Okamoto, E. S. Choi, H. Zhou, M. Briggeman, P. Irvin, A. R. Lupini, Y.-Y. Pai, E. Skoropata, C. Sohn, H. Li, H. Miao, B. Lawrie, W. S. Choi, G. Eres, J. Levy, and H. N. Lee, Sci. Adv. **7**, eabf9631 (2021).
[16] J. Fujioka, R. Yamada, M. Kawamura, S. Sakai, M. Hirayama, R. Arita, T. Okawa, D. Hashizume, M. Hoshino, and Y. Tokura, Nat. Commun. **10**, 362 (2019).
[17] R. Yamada, J. Fujioka, M. Kawamura, S. Sakai, M. Hirayama, R. Arita, T. Okawa, D. Hashizume, T. Sato, F. Kagawa, R. Kurihara, M. Tokunaga, and Y. Tokura, npj Quantum Mater. **7**, 13 (2022).
[18] M. A. Zeb and H. Kee, Phys. Rev. B **86**, 085149 (2012).
[19] Y. Chen, H.-S. Kim, and H.-Y. Kee, Phys. Rev. B **93**, 155140 (2016).
[20] H. Zhang, K. Haule, and D. Vanderbilt, Phys. Rev. Lett. **111**, 246402 (2013).
[21] P. Liu, B. Kim, X.-Q. Chen, D. D. Sarma, G. Kresse, and C. Franchini, Phys. Rev. Mater. **2**, 075003 (2018).

[22] C. Fang, Y. Chen, H.-Y. Kee, and L. Fu, Phys. Rev. B **92**, 081201 (2015).
[23] R. Yamada, J. Fujioka, M. Kawamura, S. Sakai, M. Hirayama, R. Arita, T. Okawa, D. Hashizume, M. Hoshino, and Y. Tokura, Phys. Rev. Lett. **123**, 216601 (2019).
[24] See Supplementary material for more discussions, which includes Refs. [34-38].
[25] Y. Chen, Y. Lu, and H. Kee, Nat. Commun. **6**, 6593 (2015).
[26] J.-W. Rhim and Y. B. Kim, Phys. Rev. B **92**, 045126 (2015).
[27] D. Son and B. Spivak, Phys. Rev. B **88**, 104412 (2013).
[28] R. Reis, M. Ajeesh, N. Kumar, F. Arnold, C. Shekhar, M. Naumann, M. Schmidt, M. Nicklas, and E. Hassinger, New J. Phys. **18**, 085006 (2016).
[29] C. Biagini, D. L. Maslov, M. Y. Reizer, and L. I. Glazman, EPL **55**, 383 (2001).
[30] X.-X. Zhang and N. Nagaosa, Phys. Rev. B **95**, 205143 (2017).
[31] J.-M. Carter, V. V. Shankar, M. A. Zeb, and H.-Y. Kee, Phys. Rev. B **85**, 115105 (2012).
[32] Z. Wang, H. Weng, Q. Wu, X. Dai, and Z. Fang, Phys. Rev. B **88**, 125427 (2013).
[33] C.-L. Zhang, T. Liang, M. S. Bahramy, N. Ogawa, V. Kocsis, K. Ueda, Y. Kaneko, M. Kriener, and Y. Tokura, PNAS **118**, e2111855118 (2021).
[34] H. Nielsen and M. Ninomiya, Phys. Lett. B **130**, 389 (1983).
[35] J. Xiong, S. K. Kushwaha, T. Liang, J. W. Krizan, M. Hirschberger, W. Wang, R. J. Cava, and N. P. Ong, Science **350**, 413 (2015).
[36] C. Li, L. Wang, H. Liu, J. Wang, Z. Liao, and D. Yu, Nat. Commun. **6**, 10137 (2015).
[37] C. Zhang, S. Xu, I. Belopolski, Z. Yuan, Z. Lin, B. Tong, G. Bian, N. Alidoust, C. Lee, S. Huang, T. Chang, G. Chang, C. Hsu, H. Jeng, M. Neupane, D. Sanchez, H. Zheng, J. Wang, H. Lin, C. Zhang, H. Lu, S. Shen, T. Neupert, M. Hasan, and S. Jia, Nat. Commun. **7**, 10735 (2016).
[38] S. Liang, J. Lin, S. Kushwaha, J. Xing, N. Ni, R. J. Cava, and N. P. Ong, Phys. Rev. X **8**, 031002 (2018).